Journal of Geodesy (2020) 94:30
https://doi.org/10.1007/s00190-020-01358-8

ORIGINAL ARTICLE

A line integral approach for the computation of the potential harmonic coefficients of a constant density polyhedron

Olivier Jamet[1,2] · **Dimitrios Tsoulis**[3]

Received: 18 July 2019 / Accepted: 29 January 2020 / Published online: 17 February 2020

Abstract
A novel approach for the computation of the spherical harmonic coefficients of the gravity field of a constant density polyhedron is presented. The proposed method is based on the expression of these coefficients as the volume integral of solid harmonics. It is well known that the divergence theorem leads to an expression of these volume integrals as surface integrals. We show that these surface integrals can be expressed as the sum of line integrals along the edges of the polyhedron. In contrast to previous approaches, the values of the spherical harmonic coefficients at a given degree and order result directly from the computation of the line integrals. The performed numerical implementation revealed the stability of the proposed algorithm up to degree 360 for a prismatic test source.

Keywords Gravitational potential · General polyhedron · Spherical harmonics · Numerical integration

1 Introduction

The spherical harmonic decomposition of the gravitational potential of the general polyhedron is of interest for several applications. First, it offers an analytical expression that may allow speeding up mass computation of the potential and its derivatives. Secondly, it permits a frequency domain representation that allows a direct spatial filtering of the gravitational effect of the given polyhedron. These properties are valuable in various fields. In planetary sciences, the comparison between the gravity field of a constant density body and its in-orbit determination is only possible at the observed resolution. It is thus made easier through spherical harmonic analysis (e.g., Miller et al. 2002). In geophysics, where spatial filtering has proven for long to help with source interpretation (e.g., Pawlowski and Hansen 1990), frequency domain forward modeling can be a valuable tool. In geodesy, band-limited forward modeling of the gravitational effect of the terrain serves, for instance, geoid computation in the frame of remove-restore methods (Forsberg 1993). Spatial frequency domain forward modeling of specific structures can enhance the local accuracy in these procedures.

The problem of computing the spherical harmonic coefficients of the gravity field of a constant density polyhedron has been considered by many contributions in the past. First computations, based on the series expansion of the surface of the body itself, were implemented as early as 1989 (Chao and Rubincam 1989; Martinec et al. 1989; Balmino 1994). These approaches are efficient but poorly adapted to isolated bodies away from the origin of the reference frame, such as geological layers.

The numerical computation of the coefficients through explicit integration has also been tackled very early. The first solution was proposed by Werner (1997). His strategy was based on the decomposition of the body into tetrahedra and of the integrands into homogeneous monomials that can be integrated analytically. Recent works proposed also a generalized algorithm for integrating homogeneous polynomials inside a space of any dimension (De Loera et al. 2013). However, the complexity of this family of approaches, which is of the order of n^4 to compute all the coefficients at degree and order n, does not allow very high-degree expansions.

✉ Olivier Jamet
Olivier.Jamet@ign.fr

Dimitrios Tsoulis
tsoulis@auth.gr

1 Université de Paris, Institut de physique du globe de Paris, CNRS, IGN, 75005 Paris, France

2 ENSG-Géomatique, IGN, 77455 Marne-la-Valleé, France

3 Department of Geodesy and Surveying, School of Rural and Surveying Engineering, Aristotle University of Thessaloniki, Univ Box 440, 54 124 Thessaloníki, Greece

Another family of approaches was initiated by Jamet and Thomas (2004) who proposed a linear recurrent scheme, of complexity n^2 for the computation of all the coefficients at degree and order n. This algorithm is also based on the division of the polyhedron into tetrahedra. In each tetrahedron, the volume integrals are transformed into surface integrals thanks to the divergence theorem, and the surface integrals at degree n are expressed as a function of the surface integrals at degree $n-1$ and of line integrals. This method was implemented by Tsoulis et al. (2009), who proved that it was unstable, but that it allowed the computation of the coefficients up to degree 60 for a test asteroid model. Recently, the work of Tsoulis et al. (2009) was further developed by Chen et al. (2019), who stabilized the recurrent computation by choosing a specific frame for each face and extended the approach to linearly varying densities.

The aforementioned works take benefit from the fact that the involved integrands are homogeneous functions. The application of the divergence theorem to these functions in 3 dimensions is indeed a particular case of a general property of homogeneous functions, which allows their volume integration through the integration over the volume's surface, irrespective of the dimension of the considered space (Lasserre 1999). In this work, we show that, in three-dimensional spaces, the specific properties of the integrands allow to transform the volume integrals that express the polyhedral potential harmonic coefficients, into line integrals without the need of a recurrence relation for their numerical evaluation. These findings provide the basis for a new computational approach.

After presenting the adopted notations (Sect. 2), we propose a comprehensive outline of the proposed method (Sect. 3). Section 4 gives the analytical expressions of the involved integrals. These expressions are then tested through numerical experiments (Sect. 5).

2 Notations

In the present work, we consider the general polyhedral source illustrated in Fig. 1.

The problem we are addressing was exposed previously by Tsoulis et al. (2009). The spherical harmonic decomposition of the gravitational potential $V(r,\theta,\lambda)$ of a polyhedral body $\mathcal{U}$ is defined by a set of coefficients $(C_{n,m}, S_{n,m})$ as

$$V(r,\theta,\lambda) = \frac{GM}{r}\left\{1 + \sum_{n=1}^{+\infty}\left(\frac{a}{r}\right)^n \times \sum_{m=0}^{n} P_{n,m}(\cos\theta)\left[C_{n,m}\cos(m\lambda) + S_{n,m}\sin(m\lambda)\right]\right\} \quad (1)$$

where G is the gravitational constant, M the total mass of the body and a the radius of a sphere centered at the origin that encompasses all gravitating masses. (r,θ,λ) are the spherical coordinates of the field point (radius, colatitude and longitude, respectively, with respect to the coordinate origin O, according to Fig. 1), and $P_{n,m}$ are the Legendre polynomials (for $m=0$) or associated Legendre functions (for $m>0$) as defined by Heiskanen and Moritz (1967, pp. 22–25).

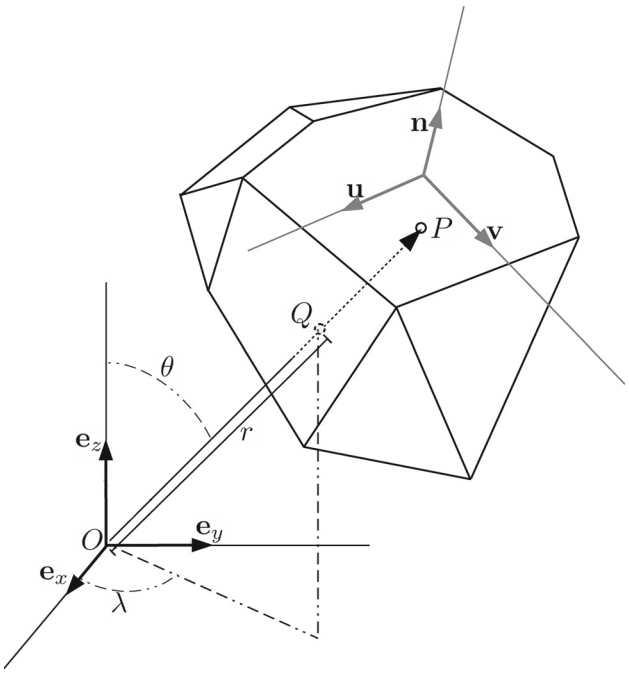

Fig. 1 A polyhedron and its associated coordinate frames

As stated for instance in Werner (1997), the coefficients $(C_{n,m}, S_{n,m})$ can be expressed as

$$\begin{bmatrix} C_{n,m} \\ S_{n,m} \end{bmatrix} = \frac{2-\delta_{0,m}}{Ma^n}\frac{(n-m)!}{(n+m)!}\iiint_{\mathcal{U}} \rho(Q)\begin{bmatrix} h^c_{n,m}(Q) \\ h^s_{n,m}(Q) \end{bmatrix} \mathrm{d}u(Q) \quad (2)$$

where $\mathrm{d}u(Q)$ is the volume element of the total volume $\mathcal{U}$ at point Q, $\rho(Q)=\rho$ is the constant density of the polyhedron, and where the functions $h^c_{n,m}$ and $h^s_{n,m}$ are defined as

$$h^c_{n,m}(r,\theta,\lambda) = r^n P_{n,m}(\cos\theta)\cos(m\lambda) \quad (3)$$

$$h^s_{n,m}(r,\theta,\lambda) = r^n P_{n,m}(\cos\theta)\sin(m\lambda) \quad (4)$$

Let us denote $h_{n,m}$ any of the $h^c_{n,m}$ or $h^s_{n,m}$ functions. In the following, we denote vectors with a boldface typesetting. Tsoulis et al. (2009) showed that the integral of $h_{n,m}$ over the volume $\mathcal{U}$ could be expressed as a surface integral through the relation

$$\begin{aligned}\iiint_{\mathcal{U}} h_{n,m}(Q)\mathrm{d}u(Q) &= \frac{1}{n+3}\oiint_{\partial\mathcal{U}} h_{n,m}(P)\mathbf{r}(P)\cdot\mathrm{d}\mathbf{S}(P)\\ &= \frac{1}{n+3}\sum_{\mathcal{F}\in\partial\mathcal{U}}\iint_{\mathcal{F}} h_{n,m}\mathbf{r}\cdot\mathbf{n}\mathrm{d}S\\ &= \frac{1}{n+3}\sum_{\mathcal{F}\in\partial\mathcal{U}} d_{\mathcal{F}}\iint_{\mathcal{F}} h_{n,m}\mathrm{d}S \qquad (5)\end{aligned}$$

where P is a point of the surface $\partial\mathcal{U}$, $\mathbf{r}(P)\equiv\mathbf{r}$ is the vector from the origin O to the point P, $\mathrm{d}\mathbf{S}$ is the infinitesimal vector area, $\mathbf{n}$ is the outward unitary vector normal to the surface $\partial\mathcal{U}$, $\mathrm{d}S$ is the scalar infinitesimal surface at point P (see Fig. 1), $\mathcal{F}$ is a given planar face of the polyhedron, and $d_{\mathcal{F}}$ is the algebraic distance from the origin O to the plane bearing the planar face $\mathcal{F}$: for any point P on the face $\mathcal{F}$, $d_{\mathcal{F}} = \mathbf{r}(P)\cdot\mathbf{n}_{\mathcal{F}}$, with $\mathbf{n}_{\mathcal{F}}$, the oriented unit normal vector to the face.

The problem of computing the coefficients is thus equivalent to the problem of computing, on any polyhedral face $\mathcal{F}$, the integral $I_{n,m}$ defined as

$$I_{n,m} = \iint_{\mathcal{F}} h_{n,m}\mathrm{d}S \qquad (6)$$

The natural basis of the considered $3D$ space, associated with the Cartesian coordinates (x, y, z), will be noted $(\mathbf{e}_x, \mathbf{e}_y, \mathbf{e}_z)$. For a given face $\mathcal{F}$ of the boundary of the polyhedron, the normal vector will be written $\mathbf{n}$, or $\mathbf{n}_{\mathcal{F}}$ when several faces are involved. The edges of the face $\mathcal{F}$ will be noted $\{\mathcal{E}\}_{\mathcal{E}\in\partial\mathcal{F}}$. For each edge $\mathcal{E}$, the leading unit oriented vector will be written $\mathbf{u}_{\mathcal{E}}$.

We will use the ∇ operator as usual in $3D$. The subscript 2 (for instance $\nabla_2 f$) will indicate that the ∇ operator is restricted to a 2-dimensional space.

3 Outline of our approach

The purpose of this section is to give a comprehensive explanation of the proposed method. A mathematical formulation is briefly presented in Sect. 4.

The proposed approach makes use of the following relation that allows to express $h_{n,m}$ as a partial derivative of $h_{n+1,m}$ (see demonstration in Appendix, "Derivative of $h_{n,m}$ along the z-axis" section).

$$\nabla h_{n+1,m}\cdot\mathbf{e}_z = \frac{\partial h_{n+1,m}}{\partial z} = (n+m+1)\,h_{n,m} \qquad (7)$$

Expressed that way, the integral is first decomposed into two parts, one using the derivative along the normal to the face, and the second one using the derivative along a vector parallel to the face. These two parts are shown to be easily expressed as sums of line integrals.

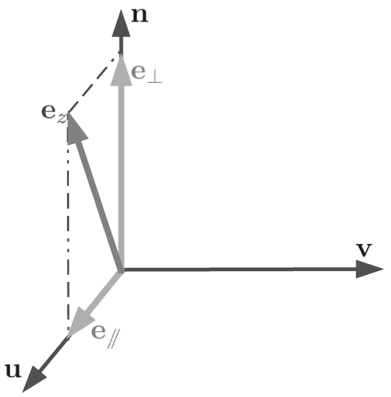

Fig. 2 Decomposition of the unit vector $\mathbf{e}_z$ into two parts: $\mathbf{e}_\perp$, perpendicular to the face, and $\mathbf{e}_{/\!/}$, parallel to the face

3.1 Decomposition

$\mathcal{F}$ being a planar face of normal unitary vector $\mathbf{n}$, the vector $\mathbf{e}_z$ can be decomposed on the whole integration domain as

$$\mathbf{e}_z = \mathbf{e}_\perp + \mathbf{e}_{/\!/} \qquad (8)$$

where $\mathbf{e}_\perp$ is orthogonal to the plane bearing the face $\mathcal{F}$, and $\mathbf{e}_{/\!/}$ is parallel to this plane (Fig. 2). These two components of $\mathbf{e}_z$ are thus defined by relation (8) and by

$$\mathbf{e}_\perp \,/\!/\, \mathbf{n} \qquad (9)$$

$$\mathbf{e}_{/\!/} \perp \mathbf{n} \qquad (10)$$

Using Eq. (7), we can express the surface integration of Eq. (6) as follows.

$$\begin{aligned}I_{n,m} &= \frac{1}{n+m+1}\iint_{\mathcal{F}}\left(\nabla h_{n+1,m}\cdot\mathbf{e}_z\right)\mathrm{d}S\\ &= \frac{1}{n+m+1}\iint_{\mathcal{F}}\left(\nabla h_{n+1,m}\cdot\left(\mathbf{e}_\perp+\mathbf{e}_{/\!/}\right)\right)\mathrm{d}S\end{aligned}$$

We thus decompose $I_{n,m}$ into two parts $I_{n,m\perp}$ and $I_{n,m/\!/}$ defined as

$$I_{n,m} = \frac{1}{n+m+1}\left(I_{n,m\perp} + I_{n,m/\!/}\right) \qquad (11)$$

$$I_{n,m\perp} = \iint_{\mathcal{F}}\nabla h_{n+1,m}\cdot\mathbf{e}_\perp\mathrm{d}S \qquad (12)$$

$$I_{n,m/\!/} = \iint_{\mathcal{F}}\nabla h_{n+1,m}\cdot\mathbf{e}_{/\!/}\mathrm{d}S \qquad (13)$$

3.2 Parallel part

The reduction of the dimension of the integral for the parallel part is straightforward. Let $(\mathbf{u}, \mathbf{v})$ be an orthonormal frame of the face $\mathcal{F}$, associated with the Cartesian coordinates (u, v), chosen so that

$$\mathbf{e}_{/\!/} = \left\|\mathbf{e}_{/\!/}\right\| \mathbf{u} \tag{14}$$

The $I_{n,m/\!/}$ integral can be written as

$$I_{n,m/\!/} = \left\|\mathbf{e}_{/\!/}\right\| \iint_{\mathcal{F}} \left(\nabla h_{n+1,m}.\right) \mathbf{u} \mathrm{d}v = \left\|\mathbf{e}_{/\!/}\right\| \iint_{\mathcal{F}} \frac{\partial h_{n+1,m}}{\partial u} \mathrm{d}u\mathrm{d}v \tag{15}$$

We then note that in the $2D$ space defined by the plane of the face $\mathcal{F}$, the derivative $\frac{\partial h_{n+1,m}}{\partial u}$ can be expressed as a divergence. Indeed

$$\nabla_2 \cdot \left(h_{n+1,m}\mathbf{u}\right) = \nabla_2 h_{n+1,m} \cdot \mathbf{u} + h_{n+1,m} \nabla_2 \cdot \mathbf{u} = \frac{\partial h_{n+1,m}}{\partial u} \tag{16}$$

since the divergence $\nabla_2 \mathbf{u}$ vanishes because $\mathbf{u}$ is constant. The integral can then be expressed as a flux through the boundary of the face, that is through its edges.

We give the expression of this sum of line integrals along the edges of $\mathcal{F}$ in Sect. 4.

3.3 Orthogonal part

The expression of the orthogonal part is due to the fact that function $h_{n+1,m}$ is harmonic. $I_{n,m\perp}$ can be expressed as the flux of $\nabla h_{n+1,m}$ through the face $\mathcal{F}$. Indeed, since $\mathbf{e}_\perp$ is orthogonal to the face, we have

$$\mathbf{e}_\perp = (\mathbf{e}_\perp \cdot \mathbf{n})\, \mathbf{n}$$

and thus

$$I_{n,m\perp} = (\mathbf{e}_\perp \cdot \mathbf{n}) \iint_{\mathcal{F}} \nabla h_{n+1,m} \cdot \mathbf{n}\, \mathrm{d}S = (\mathbf{e}_\perp \cdot \mathbf{n}) \iint_{\mathcal{F}} \nabla h_{n+1,m} \cdot \mathrm{d}\mathbf{S} \tag{17}$$

Let $\{\mathcal{E}\}_{\mathcal{E}\in\partial\mathcal{F}}$ be the set of the edges of $\mathcal{F}$. For each edge $\mathcal{E}$, let us consider the triangular face $(O, \mathcal{E})$ defined by the origin O of the frame and the edge itself, as shown in Fig. 3. Let us consider the polyhedron $\mathcal{V}_\mathcal{F}$ defined by the set of faces $\left\{\mathcal{F}, \{(O, \mathcal{E})\}_{\mathcal{E}\in\partial\mathcal{F}}\right\}$.

Since $h_{n+1,m}$ is harmonic, it will hold

$$\oiint_{\partial\mathcal{V}_\mathcal{F}} \nabla h_{n+1,m} \cdot d\mathbf{S} = 0 \tag{18}$$

where $\partial\mathcal{V}_\mathcal{F}$ is the whole surface of the volume $\mathcal{V}_\mathcal{F}$ associated with face $\mathcal{F}$

$$\partial\mathcal{V}_\mathcal{F} \equiv \left\{\mathcal{F}, \{(O, \mathcal{E})\}_{\mathcal{E}\in\partial\mathcal{F}}\right\} \tag{19}$$

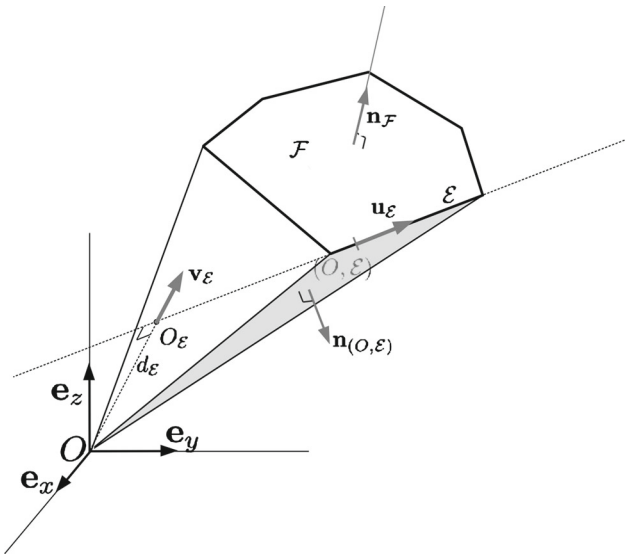

Fig. 3 Volume $\mathcal{V}_\mathcal{F}$ associated with face $\mathcal{F}$

As a consequence

$$\begin{aligned}\iint_{\mathcal{F}} \nabla h_{n+1,m} \cdot \mathrm{d}\mathbf{S} &= -\sum_{\mathcal{E}\in\partial\mathcal{F}} \iint_{(0,\mathcal{E})} \nabla h_{n+1,m} \cdot \mathrm{d}\mathbf{S} \\ &= -\sum_{\mathcal{E}\in\partial\mathcal{F}} \iint_{(0,\mathcal{E})} \nabla h_{n+1,m} \cdot \mathbf{n}_{(0,\mathcal{E})} \mathrm{d}S\end{aligned} \tag{20}$$

where $\mathbf{n}_{(0,\mathcal{E})}$ is the outward normal vector of the face $(0, \mathcal{E})$ (Fig. 3) and $\mathrm{d}\mathbf{S} \equiv \mathbf{n}_{(0,\mathcal{E})}\mathrm{d}S$.

Let us consider $\nabla h_{n+1,m} \cdot \mathbf{n}$ as a function defined in the plane of the face $(O, \mathcal{E})$, expressed in Cartesian coordinates as

$$\nabla h_{n+1,m} \cdot \mathbf{n}_{(0,\mathcal{E})} \equiv f(u, v) \tag{21}$$

$f(u, v)$ is a homogeneous function of degree n which allows for application of Euler's homogeneous function theorem

$$n\, f(u, v) = u\, \frac{\partial f}{\partial u} + v\, \frac{\partial f}{\partial v} \tag{22}$$

Thus, the following relation holds for any point P in face $(0, \mathcal{E})$

$$(n+2) f(P) = \nabla_2 \cdot \left(f(P) \begin{pmatrix} u \\ v \end{pmatrix} \right) = \nabla_2 \cdot (f(P)\, \mathbf{OP}) \tag{23}$$

As a consequence, each integral of the term $\left(\nabla h_{n+1,m} \cdot \mathbf{n}_{(0,\mathcal{E})}\right)$ on the right-hand side of Eq. (20) can be expressed as the flux of $(f(P)\mathbf{OP})$ through the boundary of the face $(O, \mathcal{E})$, that is as a sum of line integrals. A simple

expression of this sum of line integrals is proposed in Sect. 4 by expressing $\nabla h_{n+1,m}$ as the rotational of a vector field.

4 Analytical formulation

Vectors $\mathbf{e}_\perp$ and $\mathbf{e}_{/\!/}$ can be expressed as

$$\mathbf{e}_\perp = (\mathbf{e}_z \cdot \mathbf{n})\,\mathbf{n} \tag{24}$$

$$\mathbf{e}_{/\!/} = (\mathbf{n} \times \mathbf{e}_z) \times \mathbf{n} \tag{25}$$

4.1 Parallel part

Relation (25) leads to

$$\begin{aligned} I_{n,m/\!/} &= \iint_{\mathcal{F}} \nabla h_{n+1,m} \cdot ((\mathbf{n} \times \mathbf{e}_z) \times \mathbf{n})\,\mathrm{d}S \\ &= \iint_{\mathcal{F}} \left(\nabla h_{n+1,m} \times (\mathbf{n} \times \mathbf{e}_z)\right) \cdot \mathbf{n}\mathrm{d}S \end{aligned} \tag{26}$$

Since the vector $\mathbf{n} \times \mathbf{e}_z$ is constant over the face $\mathcal{F}$, we can write

$$\nabla h_{n+1,m} \times (\mathbf{n} \times \mathbf{e}_z) = \nabla \times \left(h_{n+1,m}\,(\mathbf{n} \times \mathbf{e}_z)\right) \tag{27}$$

By applying the Kelvin–Stokes theorem, we have

$$\begin{aligned} I_{n,m/\!/} &= \oint_{\partial\mathcal{F}} \left(h_{n+1,m}\,(\mathbf{n} \times \mathbf{e}_z)\right) \cdot \mathbf{dL} \\ &= \sum_{\mathcal{E}\in\partial\mathcal{F}} \int_{\mathcal{E}} h_{n+1,m}\,(\mathbf{n} \times \mathbf{e}_z) \cdot \mathbf{u}_{\mathcal{E}}\mathrm{d}L \\ &= \sum_{\mathcal{E}\in\partial\mathcal{F}} \left[\mathbf{n}, \mathbf{e}_z, \mathbf{u}_{\mathcal{E}}\right] \int_{\mathcal{E}} h_{n+1,m}\mathrm{d}L \end{aligned} \tag{28}$$

where $\mathbf{dL} \equiv \mathbf{u}_{\mathcal{E}}\mathrm{d}L$ is the elementary length vector along edge $\mathcal{E}$ and $\left[\mathbf{n}, \mathbf{e}_z, \mathbf{u}_{\mathcal{E}}\right]$ is the triple product between these three vectors, defined as the determinant of the matrix composed by their corresponding components.

4.2 Orthogonal part

The proposed expression of the orthogonal part results from the following property of $\nabla h_{n,m}$ (see Appendix, "Gradient of $h_{n,m}$ as a rotational")

$$(n+1)\,\nabla h_{n,m} = \nabla \times \left(\nabla \times \left(h_{n,m}\mathbf{r}\right)\right) \tag{29}$$

where $\mathbf{r} \equiv \mathbf{OP}$ denotes the vector from the origin to any point P of the face.

As a consequence, denoting elementary surface and line elements as in the previous sections and using relation (24), we can write

$$I_{n,m\perp} = \frac{(\mathbf{e}_z \cdot \mathbf{n})}{n+2} \iint_{\mathcal{F}} \nabla \times \left(\nabla \times \left(h_{n+1,m}\mathbf{r}\right)\right) \cdot \mathbf{dS} \tag{30}$$

and, in application of the Kelvin–Stokes theorem

$$\begin{aligned} I_{n,m\perp} &= \frac{(\mathbf{e}_z \cdot \mathbf{n})}{n+2} \oint_{\partial\mathcal{F}} \left(\nabla \times \left(h_{n+1,m}\mathbf{r}\right)\right) \cdot \mathbf{dL} \\ &= \frac{(\mathbf{e}_z \cdot \mathbf{n})}{n+2} \sum_{\mathcal{E}\in\partial\mathcal{F}} \int_{\mathcal{E}} \left(\nabla h_{n+1,m} \times \mathbf{r}\right) \cdot \mathbf{u}_{\mathcal{E}}\mathrm{d}L \\ &= \frac{(\mathbf{e}_z \cdot \mathbf{n})}{n+2} \sum_{\mathcal{E}\in\partial\mathcal{F}} \int_{\mathcal{E}} \nabla h_{n+1,m} \cdot (\mathbf{r} \times \mathbf{u}_{\mathcal{E}})\,\mathrm{d}L \end{aligned} \tag{31}$$

Let $O_{\mathcal{E}}$ be the nearest point from the origin O of the line bearing the edge $\mathcal{E}$ (Fig. 3), $d_{\mathcal{E}}$ the distance from the origin O to this line and $\mathbf{v}_{\mathcal{E}}$ the unit vector of direction $\mathbf{OO}_{\mathcal{E}}$

$$d_{\mathcal{E}} \equiv \|\mathbf{OO}_{\mathcal{E}}\| \tag{32}$$

$$\mathbf{v}_{\mathcal{E}} \equiv \begin{cases} \frac{1}{d_{\mathcal{E}}}\mathbf{OO}_{\mathcal{E}} & \text{if } d_{\mathcal{E}} > 0 \\ \mathbf{0} & \text{if } d_{\mathcal{E}} = 0 \end{cases} \tag{33}$$

The cross-product $(\mathbf{r} \times \mathbf{u}_{\mathcal{E}})$ is constant along the edge and can be expressed as

$$\mathbf{r} \times \mathbf{u}_{\mathcal{E}} = d_{\mathcal{E}}\,(\mathbf{v}_{\mathcal{E}} \times \mathbf{u}_{\mathcal{E}})$$

Thus, the orthogonal part can be expressed as a weighted sum of line integrals of the derivative of h_{n+1} along the constant (but edge dependent) direction $\mathbf{v}_{\mathcal{E}} \times \mathbf{u}_{\mathcal{E}}$

$$I_{n,m\perp} = \frac{(\mathbf{e}_z \cdot \mathbf{n})}{n+2} \sum_{\mathcal{E}\in\partial\mathcal{F}} d_{\mathcal{E}} \int_{\mathcal{E}} \nabla h_{n+1,m} \cdot (\mathbf{v}_{\mathcal{E}} \times \mathbf{u}_{\mathcal{E}})\,\mathrm{d}L \tag{34}$$

5 Numerical implementation

5.1 Outline of the implementation

A prototype software implementing the method based on the relations given in Sect. 4 was written in the interpreted language Python (van Rossum and Drake 2011).

Coordinates (x, y, z) were normalized by the reference radius a: $(x', y', z') \equiv (x/a, y/a, z/a)$. Legendre functions were normalized with the usual normalization factor following Heiskanen and Moritz (1967, p. 31)

$$N_{n,m} = \sqrt{(2 - \delta_{0,m})\,(2n+1)\,\frac{(n-m)!}{(n+m)!}} \tag{35}$$

All the used relations were adapted to the computation of the normalized coefficients

$$\begin{bmatrix} \overline{C_{n,m}} \\ \overline{S_{n,m}} \end{bmatrix} = \begin{bmatrix} C_{n,m}/N_{n,m} \\ S_{n,m}/N_{n,m} \end{bmatrix} \tag{36}$$

through the integration of

$$\overline{h_{n,m}}\left(x', y', z'\right) = \frac{N_{n,m}}{a^n} h_{n,m}\left(x, y, z\right) \tag{37}$$

Line integrals were computed through the decimation of each edge of the test body into 2^k segments, the computation of $\overline{h_{n,m}}$ and its derivatives at the $2^k + 1$ points of these segments, and the use of Romberg's integration method (Romberg 1955) as implemented in the scipy.integrate package of Python (function romb()). The exponent k was chosen as a function of the maximum computed spherical harmonic degree $n_{\max}$, the length l of the considered edge and an average distance $\overline{d}$, such as

$$\frac{l}{2^k} \leq \frac{1}{2}\frac{\pi}{n_{\max}}\overline{d} \tag{38}$$

$\overline{d}$ is defined as the average of the distances to the origin of the frame of (i) the extremities of the edge and (ii) its leading straight line. In this formula, $\pi\overline{d}/n_{\max}$ gives a raw approximate value of the resolution of the spherical harmonic model on the considered edge. The factor $1/2$ aims at dividing the edge into small intervals far beyond this resolution. A detailed description of this implementation is given in Appendix, "Implemented algorithm" section.

5.2 Test body and reference values

We chose as test body a cube of size 1000 m, centered on the point (1500, 1500, 1500) and rotated by 13 degrees around the diagonal passing through the origin (Fig. 4). The cube was located away from the center of the frame and rotated to avoid symmetries that would cause many spherical harmonic coefficients to vanish. The density of the cube was arbitrarily set to 2.67 g cm^{-3}.

The computed spherical harmonic series were compared to the value of the potential and of the gravity at point P, located at the furthest corner from the origin (see Fig. 4) and at a few other points along direction OP. The distance OP was chosen as the reference radius a for the computation of the spherical harmonic coefficients, which sets $a = \sqrt{3 \times 2000^2} = 2\sqrt{3} \times 10^3$. The point P was chosen at a corner in order to test a region of the space where high spatial frequencies are important.

The potential V_{cube} and the modulus of the gravitational attraction g_{cube} of the cube at test points were derived from the exact formulas for the prism (Nagy et al. 2000). For point P we derived the limit of the expression given by Nagy et al. when the computation point approaches corner P. The obtained reference values for P are

$$V_{\text{cube}}(t) = G\rho\left(3\log\left(\frac{1+\sqrt{3}}{\sqrt{2}}\right) - \frac{\pi}{4}\right)t^2 \tag{39}$$

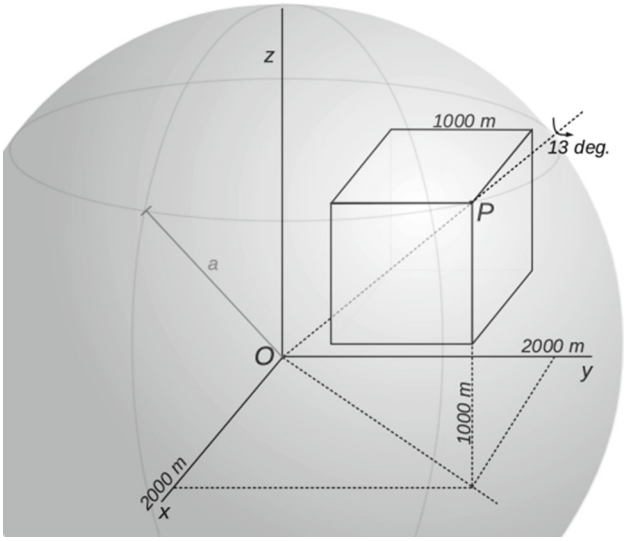

Fig. 4 Test body construction

$$g_{\text{cube}}(t) = G\rho\left(\frac{\pi}{6} + 2\log\left(\sqrt{2}\frac{1+\sqrt{2}}{1+\sqrt{3}}\right)\right)\sqrt{3}\,t \tag{40}$$

where t is the size of the cube, G the gravitational constant, and ρ the 3D density of the cube. For our given example, we had $V_{\text{cube}} = 2.120624 \times 10^{-1}\,\text{m}^2\,\text{s}^{-2}$ and $g_{\text{cube}} = 2.991996 \times 10^{-4}\,\text{m}\,\text{s}^{-2}$.

5.3 Results on simple shapes

The coefficients for our test cube were computed up to degree and order 360. The strategy adopted for splitting the edges of the cube led to 129 computation points per edge. The overall computation of the spherical harmonic coefficients took one hour and a half on a computer with 8 Gbytes of RAM and a quad-core 2.5 GHz Intel Core i7 processor.

We controlled the accuracy of the integrals on the vertical edges, for which an analytical solution is available through relation (7).

Figure 5 shows the base 10 logarithm of the relative error of the integrals on vertical edges. The relative error is computed as the modulus of the difference between the numerical value of the integrals and its reference value obtained from its analytical formula, divided by this reference value. The errors grow steadily up to nearly 100% at degree 360. We note that the adopted numerical integration strategy looks sufficient up to degree 100 to 150, but should be improved to properly handle computations at degree and order 360 or more. Nevertheless, we considered it as sufficient to test the behavior of the method up to that degree.

Table 1 shows some of the computed coefficients. The values of $\overline{C_{1,0}}$, $\overline{C_{1,1}}$ and $\overline{S_{1,1}}$ are coherent with the position of the center of mass of the cube at the 10^{-14} level of relative

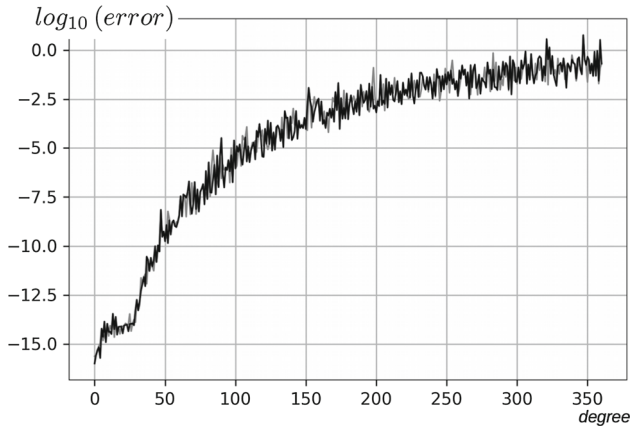

Fig. 5 $\log_{10}$ of the relative error of the $\overline{h_{n,m}}$ line integrals on the vertical edges of the cube; gray line: for $\overline{h^c_{n,m}}$; black line: for gray line: for $\overline{h^s_{n,m}}$

Table 1 Spherical harmonic coefficients of the test cube (sample)

n	m	$\overline{C_{n,m}}$	$\overline{S_{n,m}}$
1	0	2.50000000000e−01	0.0
1	1	2.50000000000e−01	2.50000000000e−01
2	0	− 6.28013820649e−15	0.0
2	1	1.45236875483e−01	1.45236875483e−01
2	2	3.86367158115e−14	1.45236875483e−01
…	…	…	…
180	0	− 1.01265250801e−08	0.0
180	2	− 7.23646197302e−12	1.48621884351e−08
…	…	…	…
360	1	− 2.52287113787e−09	− 2.51541751845e−09
360	360	− 5.51466428191e−41	5.14086641792e−40

accuracy. Indeed, the coordinates (x_c, y_c, z_c) of the center of mass of the attracting body are given by the values of the degree 1 spherical harmonic coefficients by $(x_c, y_c, z_c) = a\sqrt{3}\left(\overline{C_{11}}, \overline{S_{11}}, \overline{C_{10}}\right)$, with, in our example, $a = 2000\sqrt{3}$.

The convergence of the spherical harmonic series toward the total field value at test points was computed, starting from the corner point P (Fig. 4) and moving away along the direction OP by 1 m, 100 m, 500 m and 1 km. The total field value is given by Eqs. (39) and (40) at point P and by the prism formula proposed by Nagy et al. (2000) at other points. Figure 6 shows the convergence for the potential (a) and for the gravitational attraction modulus (b). The evolution of the values toward the full potential and attraction is steady and does not seem to show any artifact. Of course, the relative error of the series developed up to degree and order 360 is smaller for the potential value ($< 10^{-4}$ at the corner) than for its gradient ($> 10^{-2}$ at the corner) as differentiation enhances high frequencies.

This convergence compares with the behavior of the algorithm proposed by Chen et al. (2019). Figure 7 shows the convergence of the potential for the prismatic test body chosen by these authors, at the same locations as in their study. The numerical values cannot be directly compared since Chen et al. compute the potential with a varying density. Nevertheless, the overall behavior of the curve and the reached accuracy are similar, with a slightly smaller error at convergence with our method ($10^{-13.6}$ at degree 160). We note that this experiment does not allow to assess the coefficients beyond degree 150.

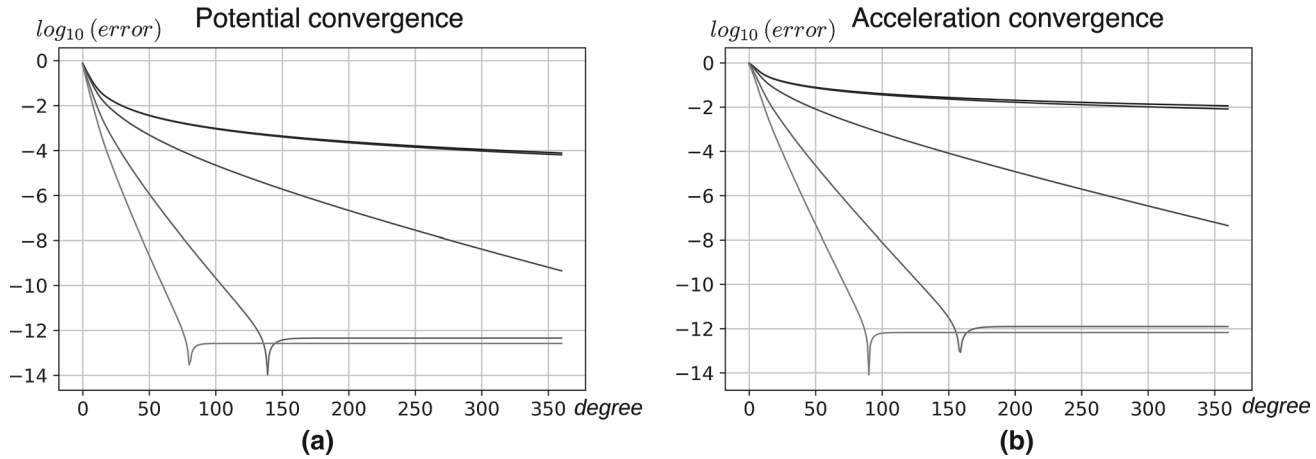

Fig. 6 Base 10 log of the difference between the total reference value and the value computed from the expansion of the spherical harmonic series up to a given degree as a function of the degree, computed at the corner P of the cube and at 5 other points along the direction (OP)—1 m, 100 m, 500 m and 1 km away; **a** on the left: gravitational potential; **b** on the right: gravitational attraction modulus; the lower is the curve, the further is the point; the first two curves (point P and 1 m from P) are nearly superimposed

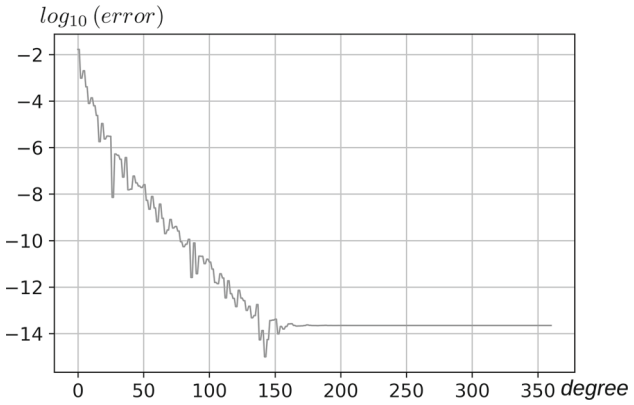

Fig. 7 Convergence of the proposed method for the test prism used in (Chen et al. 2019)

5.4 Test on a realistic body

A preliminary real size test of the method was run on an asteroid model. We chose the 1708 face model of the asteroid 433 EROS (`eros001708.tab` shape file), available at http://www.psi.edu/pds/archive/shape.html. This shape file was built after the 2002 NEAR Shoemaker probe (Domingue and Cheng 2002). It counts 1708 faces and 2562 edges. It was used in previous similar studies (Tsoulis et al. 2009; Chen et al. 2019). A basic parallel implementation of the method was set up. The computation of a 70 degree and order spherical harmonic decomposition of the potential took two hours on the same machine as previously, with four threads working in parallel. On the average, the edges were split into ten parts (11 points per edge). We assessed the quality of the decomposition through a similar experiment as in (Tsoulis et al. 2009). A set of 1000 points Q_i was randomly chosen on the reference radius sphere encompassing the body (Fig. 8). The total potential was computed at these locations using the usual analytical formulas (Tsoulis 2012).

The right part of Fig. 9 shows on a logarithmic scale the average convergence $\varepsilon(n)$ of the series toward the total value, computed as the ratio of the root-mean-square of the differences at a given degree to the root-mean-square variation of the total potential. $\varepsilon(n)$ is defined as

$$\varepsilon(n) = \sqrt{\frac{\sum_i (V_n(Q_i) - V_{\text{ref}}(Q_i))^2}{\sum_i V_{\text{ref}}(Q_i)^2}}$$

where $V_n(Q_i)$ is the series expansion of the potential truncated at degree n and $V_{\text{ref}}(Q_i)$ is the total value of the potential. Though computed only up to degree 70, this result compares favorably to the one obtained by Tsoulis et al. (2009). In this latter work, the average accuracy of the series obtained through numerical integration (Tsoulis et al. 2009, Fig. 11) appears to keep larger than 10^{-5} at degree 70, while in our test, it reaches $10^{-5.4}$. Besides, we computed, at every degree, the linear correlation coefficient between the series values $V_n(Q_i)$ and the total values $V_{\text{ref}}(Q_i)$ as in (Tsoulis et al. 2009, Fig. 12). From degree 4 up to degree 70, the correlation coefficient is greater than 0.99 and reaches 1.0–10^{-9} at degree 70 (Fig. 9b).

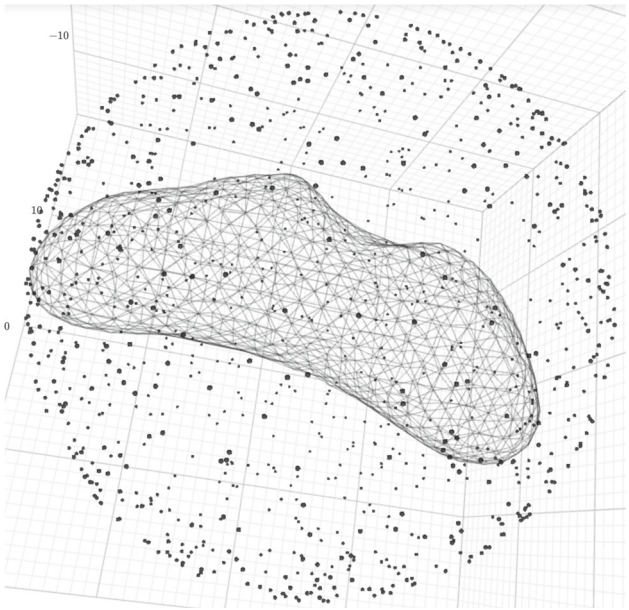

Fig. 8 433 EROS shape file: 1708 faces; 2562 edges; the set of test locations is represented by large dots when on the foreground and small ones when in the background

6 Discussion

We present a new method for computing the spherical harmonic coefficients of a general polyhedron of constant density and tested it up to degree 360 on simple shapes and up to degree 70 on a real body. We gave original analytical expressions of these coefficients as sums of line integrals. This finding avoids the necessity for either handling complex and unstable recurrent computations as in (Tsoulis et al. 2009) or splitting the body and rotating its parts as in (Chen et al. 2019).

The complexity of the proposed method ranges between the algorithm by Werner (1997), the computation burden of which varies like n^4 to get all the coefficients at degree and order n, and the one by Tsoulis et al. (2009) or Chen et al. (2019), the computation burden of which varies like n^2. In our case, the number of points computed to sample the edges of the body is of course a function of the aimed resolution and thus of the wished maximum degree. This makes theoretically the method in the order of complexity of n^3. The processing time mentioned in Sect. 5.3 was given as an indication that the computation is possible. It is not significant. Our prototype computation was handled through an

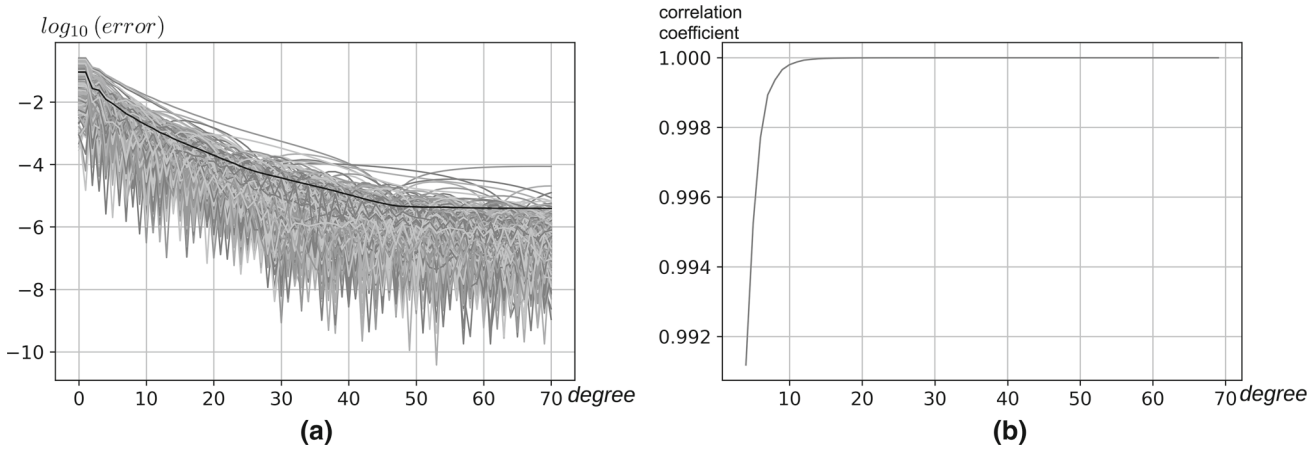

Fig. 9 (a): On the left, convergence of the spherical harmonic series representing the gravitational potential of 433 EROS: evaluation on 1000 test point; in black, the root-mean-square differences between the total values of the potential and the development at a given degree (decimal logarithm) as a function of the degree; in gray, the relative error at each of the 1000 locations (decimal logarithm). (b) On the right, correlation coefficient between the values at each test point of i) the spherical harmonic series of the potential truncated at degree n and ii) the value of the total potential, as a function of the degree n

interpreted language, and the method can of course be parallelized.

The tests presented in Sect. 5 show that our method allows to compute the spherical harmonic coefficients of a simple body at least up to degree and order 360 with a stability that compares with previous recurrent methods. The method proposed by Tsoulis et al. (2009) failed to provide accurate coefficients beyond degree 60. It was though assessed on a much more complex body. The tests presented by Chen et al. (2019) on a prism with variable density show a comparable behavior as far as accuracy is concerned. However, their results do not allow to assess the behavior of their method beyond degree 290 (Chen et al. 2019, Fig. 4, convergence of the second derivatives).

This good behavior of the convergence curves (Fig. 6) provides an evidence for a good accuracy of the coefficients in the case of a simple body. However, the method can still be improved, as our tests show also that the currently adopted line integration strategy presents some limits at high degrees. Furthermore, the chosen edge sampling strategy leads to a still very high computational cost. The computation of the decomposition for the potential of 433 EROS at degree and order 360 would require nearly 130,000 points. At this resolution, that is twice the strictly minimal number of samples necessary to represent the potential by a grid on the sphere. As a consequence, for processing an extended body, our method still does not compete with classical approaches, such as the computation of the coefficients through the convolution of a grid (Wieczorek and Meschede 2018) or through the expansion of the body surface itself into spherical harmonics (e.g., Balmino 1994). It might though be interesting for the representation in the frequency domain of local sources, such as geological structures, for which global computational schemes look inadequate.

Further work will focus on the optimization of the performance of the approach and on further numerical experiments in order to assess the accuracy of the computed coefficients, as well as the behavior of the method for complex bodies.

Acknowledgements This study was partly supported by IdEx Université de Paris ANR-18-IDEX-0001. IPGP contribution number is 4055.

Author contributions This research was jointly designed by OJ and DT; OJ found the mathematical relations and performed their implementation; and OJ and DT analyzed the results and wrote the paper.

Appendix

A.1 Derivative of $h_{n,m}$ along the z-axis

The relation expressed by Eq. (7) is obtained in polar coordinates as follows (the calculus is identical with a sin $(m\lambda)$ dependency to the longitude)

$$\begin{aligned}
&\frac{\partial h^c_{n,m}(\rho,\lambda,z)}{\partial z} \\
&= \frac{\partial}{\partial z}\left(\left(\rho^2+z^2\right)^{\frac{n}{2}} P_{n,m}\left(\frac{z}{\sqrt{\rho^2+z^2}}\right)\cos(m\lambda)\right) \\
&= \frac{\partial\left(\rho^2+z^2\right)^{\frac{n}{2}}}{\partial z} P_{n,m}\left(\frac{z}{\sqrt{\rho^2+z^2}}\right)\cos(m\lambda) \\
&\quad + \left(\rho^2+z^2\right)^{\frac{n}{2}} \frac{\partial}{\partial z} P_{n,m}\left(\frac{z}{\sqrt{\rho^2+z^2}}\right)\cos(m\lambda)
\end{aligned}$$

We have

$$\frac{\partial \left(\rho^2+z^2\right)^{\frac{n}{2}}}{\partial z} = nz\left(\rho^2+z^2\right)^{\frac{n}{2}-1}$$

and

$$\frac{\partial}{\partial z}P_{n,m}\left(\frac{z}{\sqrt{\rho^2+z^2}}\right) = \frac{1}{\sqrt{\rho^2+z^2}}\left(1-\left(\frac{z}{\sqrt{\rho^2+z^2}}\right)^2\right) .P'_{n,m}\left(\frac{z}{\sqrt{\rho^2+z^2}}\right)$$

where $P'_{n,m}$ is the first derivative of the polynomial $P_{n,m}$: $P'_{n,m}(x) = \frac{\mathrm{d}}{\mathrm{d}x}P_{n,m}(x)$.

Using the relation

$$\left(x^2-1\right)\frac{\mathrm{d}}{\mathrm{d}x}P_{n,m}(x) = nxP_{n,m}(x) - (n+m)P_{n-1,m}(x)$$

we can write

$$\frac{\partial}{\partial z}P_{n,m}\left(\frac{z}{\sqrt{\rho^2+z^2}}\right) = \frac{n+m}{\sqrt{\rho^2+z^2}}P_{n-1,m}\left(\frac{z}{\sqrt{\rho^2+z^2}}\right) -n\frac{z}{\sqrt{\rho^2+z^2}^2}P_{n,m}\left(\frac{z}{\sqrt{\rho^2+z^2}}\right)$$

and consequently

$$\frac{\partial h^c_{n,m}(\rho,\lambda,z)}{\partial z} = (n+m)\left(\rho^2+z^2\right)^{\frac{n-1}{2}}P_{n-1,m}\left(\frac{z}{\sqrt{\rho^2+z^2}}\right)\cos(m\lambda)$$

A.2 Gradient of $h_{n,m}$ as a rotational

Starting from the identity

$$\nabla\times(\nabla\times\mathbf{F}) = \nabla(\nabla\cdot\mathbf{F}) - \triangle\mathbf{F}$$

we have

$$\nabla\times\left(\nabla\times\left(h_{n,m}\mathbf{r}\right)\right) = \nabla\left(\nabla\cdot\left(h_{n,m}\mathbf{r}\right)\right) - \Delta\left(h_{n,m}\mathbf{r}\right) \quad (41)$$

From the homogeneity of $h_{n,m}$, we get, through the Euler relation

$$\nabla\cdot\left(h_{n,m}\mathbf{r}\right) = (n+3)\,h_{n,m}$$

and thus

$$\nabla\left(\nabla\cdot\left(h_{n,m}\mathbf{r}\right)\right) = (n+3)\,\nabla h_{n,m}$$

The second term of relation (41) can be written in Cartesian coordinates

$$\begin{aligned}\Delta\left(h_{n,m}\mathbf{r}\right) &= \begin{pmatrix}\triangle\left(xh_{n,m}\right)\\ \triangle\left(yh_{n,m}\right)\\ \triangle\left(zh_{n,m}\right)\end{pmatrix}\\ &= \begin{pmatrix}2\nabla h_{n,m}\cdot\mathbf{e}_x + x\triangle h_{n,m}\\ 2\nabla h_{n,m}\cdot\mathbf{e}_y + y\triangle h_{n,m}\\ 2\nabla h_{n,m}\cdot\mathbf{e}_z + z\triangle h_{n,m}\end{pmatrix}\\ &= 2\nabla h_{n,m} + \left(\triangle h_{n,m}\right)\mathbf{r}\end{aligned}$$

Since $h_{n,m}$ is harmonic, $\triangle h_{n,m} = 0$ and we get

$$\nabla\times\left(\nabla\times\left(h_{n,m}\mathbf{r}\right)\right) = (n+1)\,\nabla h_{n,m}$$

A.3 Implemented algorithm

The proposed method was implemented as follows.

First, all the coordinates of the considered body are normalized to the reference radius a (see Sect. 5.1). The numerical representation of the polyhedron is transformed into an edge-oriented representation: list of all edges $\mathcal{E}$, with the following attributes

- $\mathbf{u}_\mathcal{E}$, unitary vector of the oriented edge;
- $\mathbf{v}_\mathcal{E}$, unitary vector of the direction orthogonal to $\mathcal{E}$ and passing through the origin O
- $d_\mathcal{E}$, distance between the origin O and the line bearing the edge $\mathcal{E}$
- $A_\mathcal{E}$, $B_\mathcal{E}$, vertices of the edge
- $\mathbf{n}_{R\mathcal{E}}$, $\mathbf{n}_{L\mathcal{E}}$, unitary outward normals to, respectively, the right and the left face.

Then, for each edge $\mathcal{E}$, the integration follows three steps:

1. sampling: The sampling of the edge consists in listing $\left(2^k+1\right)$ points $\{Q_i\}_{i=0..2^k}$ regularly spaced inside the edge $A_\mathcal{E}B_\mathcal{E}$, with $Q_0 = A_\mathcal{E}$, $Q_{2^k} = B_\mathcal{E}$, and with k verifying Eq. (38); the average distance is computed as $\overline{d} = \left(d_\mathcal{E} + OA_\mathcal{E} + OB_\mathcal{E}\right)/3$
2. $h_{n,m}$ computation: At each point Q_i, for every degree n and order m, four values are computed:
   (a) $\overline{h^c_{n,m}}(Q_i)$
   (b) $\overline{h^s_{n,m}}(Q_i)$
   (c) $\nabla\overline{h^c_{n,m}}\cdot(\mathbf{v}_\mathcal{E}\times\mathbf{u}_\mathcal{E})$
   (d) $\nabla\overline{h^s_{n,m}}\cdot(\mathbf{v}_\mathcal{E}\times\mathbf{u}_\mathcal{E})$
3. Integral computation: The integral along the edge of each quantity (a), (b), (c) and (d) is computed from the list of the values at points Q_i using the Romberg algorithm

implemented in the *scipy* Python package; the integral $I_{\mathcal{E}}\left(\overline{h^c_{n,m}}\right)$ of $\overline{h^c_{n,m}}$ along edge $\mathcal{E}$ is thus obtained as

$$I_{\mathcal{E}}\left(\overline{h^c_{n,m}}\right) = \mathrm{d}l \times \text{scipy.integrate.romb}\left(\left[\overline{h^c_{n,m}}\left(Q_i\right)\right]_{i=0..2^k}\right)$$

where $\mathrm{d}l = \|\mathbf{A}_{\mathcal{E}}\mathbf{B}_{\mathcal{E}}\|/2^k$ is the distance between two consecutive samples on the edge $\mathcal{E}$.

4. Integral weighting: The computed integrals are weighted according to Eqs. (5), (28) and (34) to store them as the edge contributions to each degree and order; for instance, the parallel edge contribution $C_{L/\!/}\left(\overline{h^c_{n,m}}\right)$ to the volume integral $\overline{\iiint h_{n,,m}}$ for its left face will be computed as

$$C_{L/\!/}\left(\overline{h^c_{n,m}}\right) = \frac{d_{\mathcal{F}}}{n+3}\frac{\left[\mathbf{n}_{L\mathcal{E}}, \mathbf{e}_z, \mathbf{u}_{\mathcal{E}}\right]}{n+m+1} I_{\mathcal{E}}\left(\overline{h^c_{n+1,m}}\right)$$

with $d_{\mathcal{F}} = \mathbf{n}_{L\mathcal{E}}\cdot\mathbf{OA}_{\mathcal{E}}$. The sum $\sum_{\mathcal{E}\in\partial\mathcal{F}}\left[\mathbf{n}_{L\mathcal{E}}, \mathbf{e}_z, \mathbf{u}_{\mathcal{E}}\right] I_{\mathcal{E}}$ is the integral $I_{n,m/\!/}$ of Eq. (13). However, we do not make this face contribution explicit in our implementation because we first sum each edge contribution (from left and right face).

For each degree and order, the contributions computed at the previous step 4 are summed over all the edges; all the terms depending on $\overline{h^c_{n,m}}$ are summed together to yield a scaled coefficient $\overline{C_{n-1,m}}^*$, while all the terms depending on $\overline{h^s_{n,m}}$ will yield a scaled coefficient $\overline{S_{n-1,m}}^*$.

The ratio between the normalized coefficients, $\overline{C_{n,m}}$ and $\overline{S_{n,m}}$, and the scaled coefficients, $\overline{C_{n,m}}^*$ and $\overline{S_{n,m}}^*$, is deduced from the mathematical expression of the integrals

$$\frac{\overline{C_{n,m}}}{\overline{C_{n,m}}^*} = \frac{\sqrt{(n+m+1)}}{\sqrt{(2n+1)\,(2n+3)}\sqrt{(n-m+1)}}\frac{a^3}{V}$$

where V is the total volume of the considered polyhedron. The same relation holds for $\overline{S_{n,m}}$ and $\overline{S_{n,m}}^*$.

References

Balmino G (1994) Gravitational potential harmonics from the shape of an homogeneous body. Celest Mech Dyn Astron 60(3):331–364

Chao BF, Rubincam DP (1989) The gravitational field of Phobos. Geophys Res Lett 16(8):859–862

Chen C, Chen Y, Bian S (2019) Evaluation of the spherical harmonic coefficients for the external potential of a polyhedral body with linearly varying density. Celest Mech Dyn Astron 131(2):8

De Loera JA, Dutra B, Köppe M, Moreinis S, Pinto G, Wu J (2013) Software for exact integration of polynomials over polyhedra. Comput Geom 46:232–252

Domingue DL, Cheng AF (2002) Near earth asteroid rendezvous: the science of discovery. Johns Hopkins APL Tech Digest 23(1):6–17

Forsberg R (1993) Modelling the fine structure of the geoid: methods, data requirements and some results. Surv Geophys 14:403–418

Heiskanen WA, Moritz H (1967) Physical geodesy. WH Freeman and Company, San Fransisco

Jamet O, Thomas E (2004) A linear algorithm for computing the spherical harmonic coefficients of the gravitational potential from a constant density polyhedron. In: CNES (ed) Proceedings of the 2nd international GOCE user workshop, GOCE, the geoid and oceanography

Lasserre JB (1999) Integration and homogeneous functions. Proc Am Math Soc 127(3):813–818

Martinec Z, Pěč K, Burša M (1989) The Phobos gravitational field modeled on the basis of its topography. Earth Moon Planets 45:219–235

Miller J, Konopliv A, Antreasian P, Bordi J, Chesley S, Helfrich C, Owen W, Wang T, Williams B, Yeomans D, Scheeres D (2002) Determination of shape, gravity, and rotational state of asteroid 433 eros. Icarus 155(1):3–17

Nagy D, Papp G, Benedek J (2000) The gravitational potential and its derivatives for the prism. J Geod 74(7–8):552–560

Pawlowski RS, Hansen RO (1990) Gravity anomaly separation by Wiener filtering. Geophysics 55(5):539–548

Romberg W (1955) Vereinfachte numerische integration. Det Kongelige Norske Videnskabers Selskab Forhandlinger 28(7):30–36 Trondheim

Tsoulis D (2012) Analytical computation of the full gravity tensor of a homogeneous arbitrarily shaped polyhedral source using line integrals. Geophysics 77(2):F1–F11

Tsoulis D, Jamet O, Verdun J, Gonindard N (2009) Recursive algorithms for the computation of the potential harmonic coefficients of a constant density polyhedron. J Geod 83(10):925–942

van Rossum G, Drake FL (2011) The Python language reference manual. Network Theory Ltd, Boston

Werner RA (1997) Spherical harmonic coefficients for the potential of a constant-density polyhedron. Comput Geosci 23(10):1071–1077

Wieczorek MA, Meschede M (2018) Shtools: tools for working with spherical harmonics. Geochem Geophys Geosyst 19(8):2574–2592